Abdominal Radiology (2019) 44:2841–2851
https://doi.org/10.1007/s00261-019-02018-y

KIDNEYS, URETERS, BLADDER, RETROPERITONEUM

Can MRI be used to diagnose histologic grade in T1a (< 4 cm) clear cell renal cell carcinomas?

Kevin Moran[1] · Jorge Abreu-Gomez[2] · Satheesh Krishna[3] · Trevor A. Flood[2] · Daniel Walker[1] · Matthew D. F. McInnes[1] · Nicola Schieda[1,4]

Published online: 29 April 2019

Abstract

Objective To assess whether MRI can differentiate low-grade from high-grade T1a cc-RCC.

Materials and methods With IRB approval, 49 consecutive solid < 4 cm cc-RCC (low grade [Grade 1 or 2] $N = 38$, high grade [Grade 3] $N = 11$) with pre-operative MRI before nephrectomy were identified between 2013 and 2018. Tumor size, apparent diffusion coefficient (ADC) histogram analysis, enhancement wash-in and wash-out rates, and chemical shift signal intensity index (SI index) were assessed by a blinded radiologist. Subjectively, two blinded Radiologists also assessed for (1) microscopic fat, (2) homogeneity (5-point Likert scale), and (3) ADC signal (relative to renal cortex); discrepancies were resolved by consensus. Outcomes were studied using Chi square, multivariate analysis, logistic regression modeling, and ROC. Inter-observer agreement was assessed using Cohen's kappa.

Results Tumor size was 24 ± 7 (13–39) mm with no association to grade ($p = 0.45$). Among quantitative features studied, corticomedullary phase wash-in index ($p = 0.015$), SI index ($p = 0.137$), and tenth-centile ADC ($p = 0.049$) were higher in low-grade tumors. 36.8% (14/38) low-grade tumors versus zero high-grade tumors demonstrated microscopic fat ($p = 0.015$; Kappa = 0.67). Microscopic fat was specific for low-grade disease (100.0% [71.5–100.0]) with low sensitivity (36.8% [21.8–54.6]). Other subjective features did not differ between groups ($p > 0.05$). A logistic regression model combining microscopic fat + wash-in index + tenth-centile-ADC yielded area under ROC curve 0.98 (Confidence Intervals 0.94–1.0) with sensitivity/specificity 87.5%/100%.

Conclusion The combination of microscopic fat, higher corticomedullary phase wash-in and higher tenth-centile ADC is highly accurate for diagnosis of low-grade disease among T1a clear cell RCC.

Keywords Renal cell carcinoma · Clear cell · Grade · Magnetic Resonance Imaging · Fuhrman Nuclear Grade

✉ Nicola Schieda
nschieda@toh.ca

Kevin Moran
kmoran@toh.ca

Jorge Abreu-Gomez
jabreugomez@toh.ca

Satheesh Krishna
satheeshkrishna.jeyaraj@uhn.ca

Trevor A. Flood
taflood@toh.ca

Daniel Walker
dwalker@toh.ca

Matthew D. F. McInnes
mmcinnes@toh.ca

[1] Department of Medical Imaging, The Ottawa Hospital, Ottawa, ON, Canada

[2] Department of Anatomical Pathology, The Ottawa Hospital, Ottawa, ON, Canada

[3] Joint Department of Medical Imaging, University Health Network, The University of Toronto, Toronto, ON, Canada

[4] Department of Medical Imaging, The Ottawa Hospital, 1053 Carling Avenue, Room C159, Ottawa, ON K1Y 4E9, Canada

Introduction

Renal cell carcinoma (RCC) is the most common renal malignancy and accounts for approximately 80% of solid renal masses encountered on imaging studies [1, 2]. While RCC are typically managed radically with surgery or ablation, active surveillance (AS) of small renal masses is an increasingly popular management option especially in older patients who may not be ideal candidates for radical therapy [3–5]. The risk of metastatic disease in < 4 cm (clinical T1a) RCC is low [6]; however, RCC subtypes behave differently [7, 8]. Clear cell (cc) RCC is the most common RCC subtype and is also the most aggressive, with the highest rates of metastatic disease compared to other subtypes [7, 8]. Although AS of cT1a renal masses does not specify RCC subtype, International Guidelines regarding management of RCC now include percutaneous biopsy in the initial work-up of small renal masses acknowledging important differences in behavior and suitability for surveillance comparing clear cell to other RCC [9, 10]. Moreover, subtyping of small renal masses with MRI is becoming increasingly recognized in the Imaging and Urological literature as being highly accurate, particularly for the diagnosis of clear cell tumors [11]. Clear cell RCC are graded using the International Society of Urological Pathology (ISUP) grading system (similar to the previously used Fuhrman Nuclear Grading system), and the grade of clear cell RCC correlates strongly with adverse outcomes and survival [12, 13]. Therefore, a knowledge of grade of clear cell RCC tumor among grade cT1a masses would be ideal when determining suitability for AS.

Renal mass biopsy, though safe is not without risk and though accurate, may differ with respect to final histological diagnosis. Biopsy is accurate for diagnosis of tumor subtype; however, accuracy decreases with respect to histologic grade in biopsy specimens [14]. Previously several imaging findings on CT and MRI have been used to differentiate low-grade from high-grade RCC including quantitative apparent diffusion coefficient (ADC) metrics [15], enhancement patterns [16–18], and more recently texture analysis [19, 20]. A limitation of previous studies evaluating imaging features for grading of RCC is that they did not stratify tumors by their size, which is a fundamental criterion in the TNM staging system of RCC [21, 22]. This is particularly noteworthy in cT1a renal masses because grade of tumor is less important for management decisions in ≥ cT2 masses (tumors > 4 cm in size) where nephrectomy is generally performed unless the patient is a poor surgical candidate due substantially increased rates of metastatic disease in tumors > 4 cm [23, 24]. Grading of cT1a clear cell RCC could alter management decisions, since a surgeon may be less willing to surveil a high-grade clear cell tumor compared to a low-grade tumor. cT1a masses may also be better suited for grading with imaging because of their small size, as it is a common clinical observation at histopathological analysis that smaller tumors show more homogeneous grade throughout the tumor, whereas larger tumors commonly show areas of varying low-grade and high-grade pattern due increased intratumoral heterogeneity [23, 25, 26]. The purpose of this study is therefore to assess the ability of MRI to differentiate between low-grade and high-grade cT1a (< 4 cm) clear cell tumors using subjective and quantitative analysis of MRI.

Materials and methods

Patients

This retrospective study was approved by our research ethics board who waived the need for informed consent. Between January 2013 and July 2018, we performed a retrospective consecutive search of the pathology database from a single institution for the diagnosis of pathologically confirmed T1a clear cell renal cell carcinoma diagnosed by partial or complete nephrectomy with pre-operative MRI. We identified 74 tumors that were potentially eligible for study. From these, 14 tumors were excluded because the tumors were not solid (defined as having a > 50% cystic component on imaging), four tumors were excluded because they had been diagnosed on pre-operative MRI of the spine (which included only T1-weighted and T2-weighted sequences), two tumors were excluded because no histological grade was provided and histopathology slides could not be retrieved, one tumor was excluded because it demonstrated mixed clear

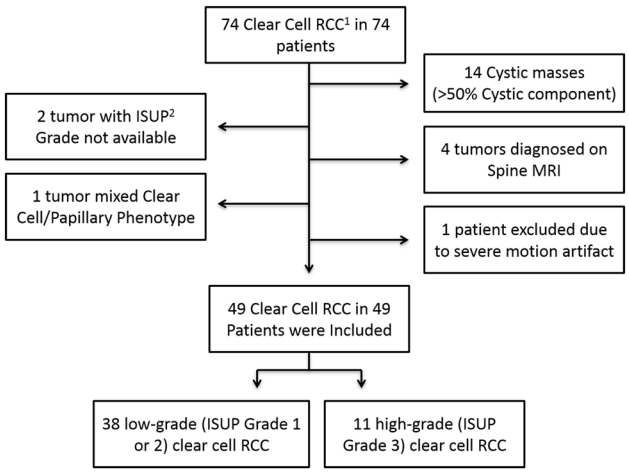

Fig. 1 Inclusion and exclusion criteria for patient selection in the current study. 1 = renal cell carcinoma, 2 = International Society of Urological Pathology

cell-papillary phenotype, and one tumor was excluded due to severe motion artifact precluding accurate assessment on MRI. After applying exclusion criteria, there were 49 solid T1a clear cell tumors in 49 patients. A summary of inclusion and exclusion criteria are provided in Fig. 1.

Histopathology

The histopathological diagnosis and grade of tumors for clear cell RCC were independently verified by a dedicated genitourinary (GU) pathologist (TAF) with 13 years of experience in GU pathology. For diagnosis of cc-RCC, the following morphological criteria were used. Tumors were characterized at hematoxylin and eosin staining and composed of varying cells with clear or eosinophilic cytoplasm and a characteristic network of small, thin walled ('chicken wire') vasculature [27]. Grading of cc-RCC was performed according to the 4-Tier International Society of Urological Pathology (ISUP) grading system where Grade 1 nucleoli are inconspicuous at ×400, Grade 2 nucleoli are prominent at ×400, nucleoli are prominent at ×100, and Grade 4 cells show nuclear pleomorphism, multinucleated giant cells, sarcomatoid and/or rhabdoid changes [27]. Using these criteria there were 38 low-grade tumors (4 Grade 1 and 34 Grade 2) and 11 high-grade tumors (11 Grade 3, 0 Grade 4).

MRI technique

In 37 out of 49 patients, MRI was performed at a single-tertiary care referral center. MRI was performed on one of three clinical 1.5 or 3 T systems (Symphony [$N=19$ patients] or TRIO [$N=8$ patients], Siemens Healthcare, Malvern PA, USA, or Discovery 750W [$N=10$ patients], General Electric Healthcare, Milwaukee WI, USA) using a torso phased-array coil (6 element anterior array for the TRIO, 4 element anterior array for the Symphony, and 16 element array for the Discovery 750W). A summary of the multi-parametric renal mass MRI protocol used at our institution at 1.5 and 3 T is provided in Table 1. For gadolinium-enhanced imaging, 3-dimensional fat-suppressed gradient-recalled echo

Table 1 Pulse sequence parameters for dual-echo T1W (in and opposed phase) GRE, T2W TSE/FSE, and volume-interpolated T1W fat-suppressed pre- and post-gadolinium-enhanced GRE at 1.5 and 3 T

Pulse sequence	Dual-echo T1W GRE			T2W TSE/FSE	Volume-interpolated T1W 3D GRE[a]		Diffusion-weighted imaging[b]
	2D GRE	3D GRE		Single-shot TSE/FSE	3T	1.5T	Single-shot echo-planar imaging
		3T	1.5T				
Physiology	Breath hold	Breath hold	Breath hold	Respiratory-triggered breath hold	Breath hold		Breath hold
Duration	21 s	16 s	20 s	3–4 min 22 s	20 s		21 s
Fat suppression	N/A	N/A	N/A	N/A	Chemical or spectral inversion recovery		Spectral inversion recovery
TE (IP/OP)[b]; TR (ms)	(4.6/2.3); 160–180	(2.5/1.3); 5.5 and (2.2/1.1); 4.0	(4.6/2.3); 7.6	83–88; 1030	1.7–2.5; 4.0–4.5	1.4; 4.3	60.8–74; 2075–4600
Flip angle (degrees)	70	10–12	10	180	10–12	10–12	90
Bandwidth (Hz)	260	700	313	450	325–460	488	250–1446
Number of excitations	1	0.7–1	1	Half-Fourier	1	1	2
Acceleration factor	2	2	1	1 2	2	2	2
Matrix size	256/320 × 134/152	294/224	192/320	170/256	256/320	132/320	130/38; 96/75
Field of view (cm)	25 × 35	25 × 35	25 × 35	25 × 35	25 × 35	25 × 35	25 × 35
Slice thickness (mm)	5–6	3–4	3–5	5	2.5–4	2.5–4	6

Imaging was performed on clinical 1.5 Tesla (Symphony or Avanto, Siemens Healthcare) or 3 Tesla (TRIO, Siemens Healthcare; Discovery 750W, General Electric Healthcare) systems

[a]VIBE (Siemens Healthcare), LAVA (General Electric Healthcare)

[b]Diffusion-weighted imaging performed with two *b* values (50 and 600 mm^2/s) with ADC map automatically derived

[c]IP = in phase, OP = opposed phase

(GRE) T1 weighted (VIBE, Siemens Healthcare or LAVA, GE Healthcare) sequences are performed dynamically after the administration of 0.1 mmol/kg of gadobutrol (Gadovist, Bayer Healthcare) injected at a rate of 2 mL/s followed by a 20 mL saline flush. Axial contrast-enhanced images were obtained following an empiric 30–40-s delay followed by successive acquisitions every minute for 3–5 min. The first axial sequence (obtained at 30–40 s) was used as the corticomedullary phase and the second axial sequence (obtained at 60–80 s) was used as the nephrographic phase. The 3-min equilibrium phase was considered as the delayed phase since a 5-min delay was not performed in all patients. Diffusion-weighted imaging (DWI) was performed using either a breath-hold or respiratory-triggered fat-suppressed single-shot echo-planar sequence with tri-directional gradients and low ($b = 50$ mm^2/s) and high ($b = 600$ mm^2/s) b values for automatic derivation of apparent diffusion coefficient (ADC) map using a standard monoexponential model.

In the remaining 12 patients, MRI was performed at peripheral institutions within our regional LHIN using clinical 1.5 Tesla systems (Avanto or Aera [$N = 6$ patients]; Siemens Healthcare, Achieva [$N = 4$ patients]; and Philips Healthcare and Optima 450W [$N = 2$ patients], GE Healthcare) with studies available to review through our PACS server. Torso phased-array coil was used (6 element array for Avanto and 4 element array for Achieva and Signa). MRI technique was similar to that used at the single-tertiary care center with similar sequence parameters and dynamic acquisition technique (including injection parameters and timing of acquisition) for 3-dimensional fat-suppressed GRE. Gadobutrol (Gadovist, Bayer Healthcare) was also used with a dose of 0.1 mmol/kg. Choice of *b* value for DWI varied slightly but always included both low (0–100 mm^2/s) and high (500–800 mm^2/s) *b* values for ADC calculation.

Subjective analysis

Image analysis was performed using a standard Picture Archiving and Communication System (PACS; Horizon Medical Imaging, McKesson Corporation). Two blinded genitourinary radiologists with 12 and 7 years of experience (NS and JAG) evaluated MRI for the following features: (1) homogeneity using nephrographic phase-enhanced images [5-point Likert-type scale where 1 = completely homogeneous (uniform signal intensity), 2 = mostly homogeneous, 3 = mixed areas of homogeneous and heterogeneous signal intensity, 4 = mostly heterogeneous, and 5 = completely heterogeneous (mixed areas of low and high signal intensity)] as described previously [28], (2) microscopic fat, which in clear cell RCC is due to the presence of fat molecules within tumor cells [29], by noting a signal intensity drop on OP compared to IP chemical shift MRI (binary outcome: present or absent), and (3) signal intensity of solid components on ADC map images relative to the ipsilateral renal cortex. Solid components on ADC were determined by cross-referencing with areas showing enhancement on gadolinium-enhanced delayed phase images. For homogeneous tumors, the overall signal was assessed and for heterogeneous tumors the darkest area on ADC was evaluated and compared to ipsilateral normal renal cortex (3-point scale; hypointense, isointense, hyperintense), Figs. 2 and 3. Discrepancies in subjective interpretation for statistically significant variables were later resolved by consensus review by the two radiologists who remained blinded to pathological outcomes after their initial independent blinded review.

Quantitative analysis

One of the abdominal radiologists (JAG) also measured signal intensity values using region of interest (ROI) analysis and segmented tumors for quantitative histogram analysis after performing subjective interpretation of each lesion.

Chemical shift signal intensity index

An ROI was placed in the lesion avoiding the edges of the lesion to not include areas of chemical shift artifact of the second kind in the measurement [30]. For tumors not showing any signal intensity drop on opposed-phase (OP) compared to in-phase (IP) images, an ROI was placed on the axial image containing the most solid components encompassing 2/3 of the area of the solid component of the mass. The solid component of the mass, which was used for all quantitative measurements, was determined by cross-referencing to areas of enhancement determined on the delayed phase-enhanced MRI, Figs. 2 and 3. For tumors showing a signal intensity drop on OP compared to IP images, an ROI was placed encompassing 2/3 of the area subjectively showing signal intensity drop and measuring at least 5 mm in diameter, Fig. 3. A fixed diameter (10 mm) ROI was also placed in the spleen at the same level on IP and OP images. Chemical shift SI index (SI index) and chemical shift tumor-to-spleen SI ratio (SIR) were calculated as follows: ((SI tumor IP − SI tumor OP)/SI tumor IP) and ((SI tumor OP/SI spleen OP)/(SI tumor IP/SI tumor OP)) [31–33].

Gadolinium-enhanced wash-in and wash-out indices

For gadolinium-enhanced images, ROIs were also placed on the axial image where the tumor contained the most solid enhancing components, Figs. 2 and 3. For homogeneously enhancing tumors, an ROI encompassing 2/3 of the circumference of the enhancing portion of the mass was placed on the corticomedullary and nephrographic phase-enhanced images and copied onto the pre-contrast images. For heterogeneously enhancing tumors, an ROI was placed

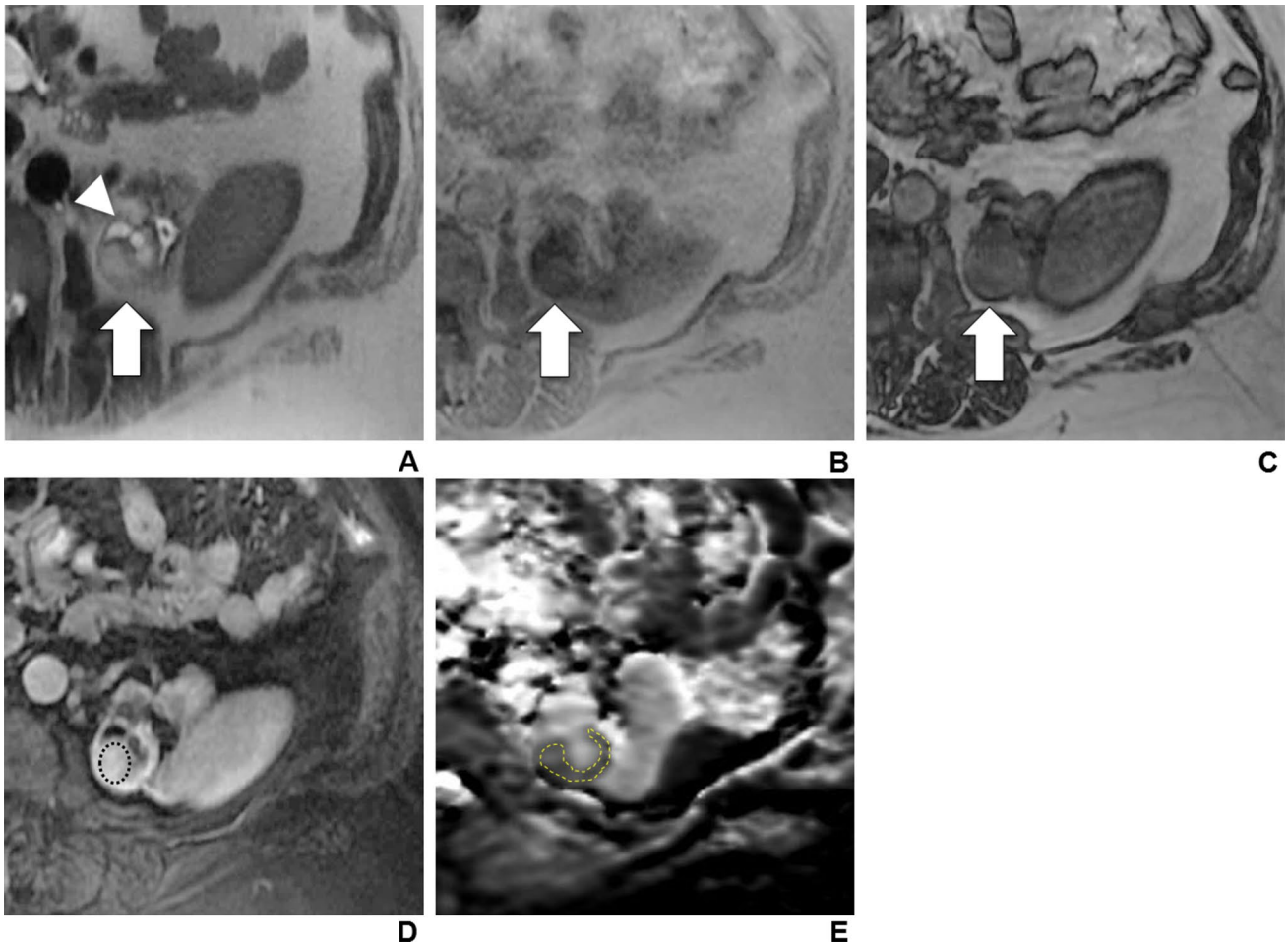

Fig. 2 A 74-year-old male with high-grade (ISUP Grade 3) clear cell RCC. **a** Axial T2-weighted (T2W) image shows a heterogeneously hyperintense mass in the upper pole of the left kidney (white arrow) with minimal peripheral cystic change or necrosis (arrowhead). **b**, **c** Axial T1-weighted (T1W) in- and opposed-phase images show the absence of any microscopic fat (arrows) due to absent signal intensity drop on opposed-phase images. **d** Axial fat-suppressed (FS) T1W post-gadolinium-enhanced image obtained in the corticomedullary phase depicts moderate enhancement. The circular region of interest (ROI; black dotted circle) depicts the method of measurement of signal intensity. The axial slice which contained the most solid enhancing components was used and a circular ROI was placed encompassing 2/3 of the solid enhancing component avoiding areas of necrosis and cystic change. **e** Axial apparent diffusion coefficient (ADC) map image shows marked low signal in the solid components of the mass. A custom fit region of interest was placed (yellow dotted ROI) encompassing the solid components of the tumor, by cross-referencing the ADC map image with the enhanced T1W images. In this way, mean, 25th and tenth-centile ADC values were extracted

encompassing 2/3 of the area subjectively showing maximal enhancement on the corticomedullary phase measuring at least 5 mm in diameter. This ROI was then copied onto the nephrographic and pre-contrast phase images. Using the ROI measurements from the pre-contrast, corticomedullary and nephrographic phase images, tumor wash-in ([[Corticomedullary phase signal intensity − Pre-contrast phase signal intensity]/Pre-contrast phase signal intensity] × 100) and wash-out ([[Nephrographic phase signal intensity/Corticomedullary phase signal intensity]/Corticomedullary phase signal intensity] × 100) were calculated as described previously [34, 35].

ADC analysis

On ADC map images, ADC metrics were measured on the axial image that contained the most solid enhancing components. The axial image used for ROI measurement was exported (after patient-identifying information was removed) in DICOM format from PACS to an independent workstation for lesion analysis using Image J (version 1.48, National Institutes of Health). Each image was segmented by the Radiologist to encompass as much of the solid enhancing tumor as possible avoiding extra-tumoral structures and areas of cystic change and necrosis. ADC histogram analysis (mean, 25th and 10th centiles) were extracted.

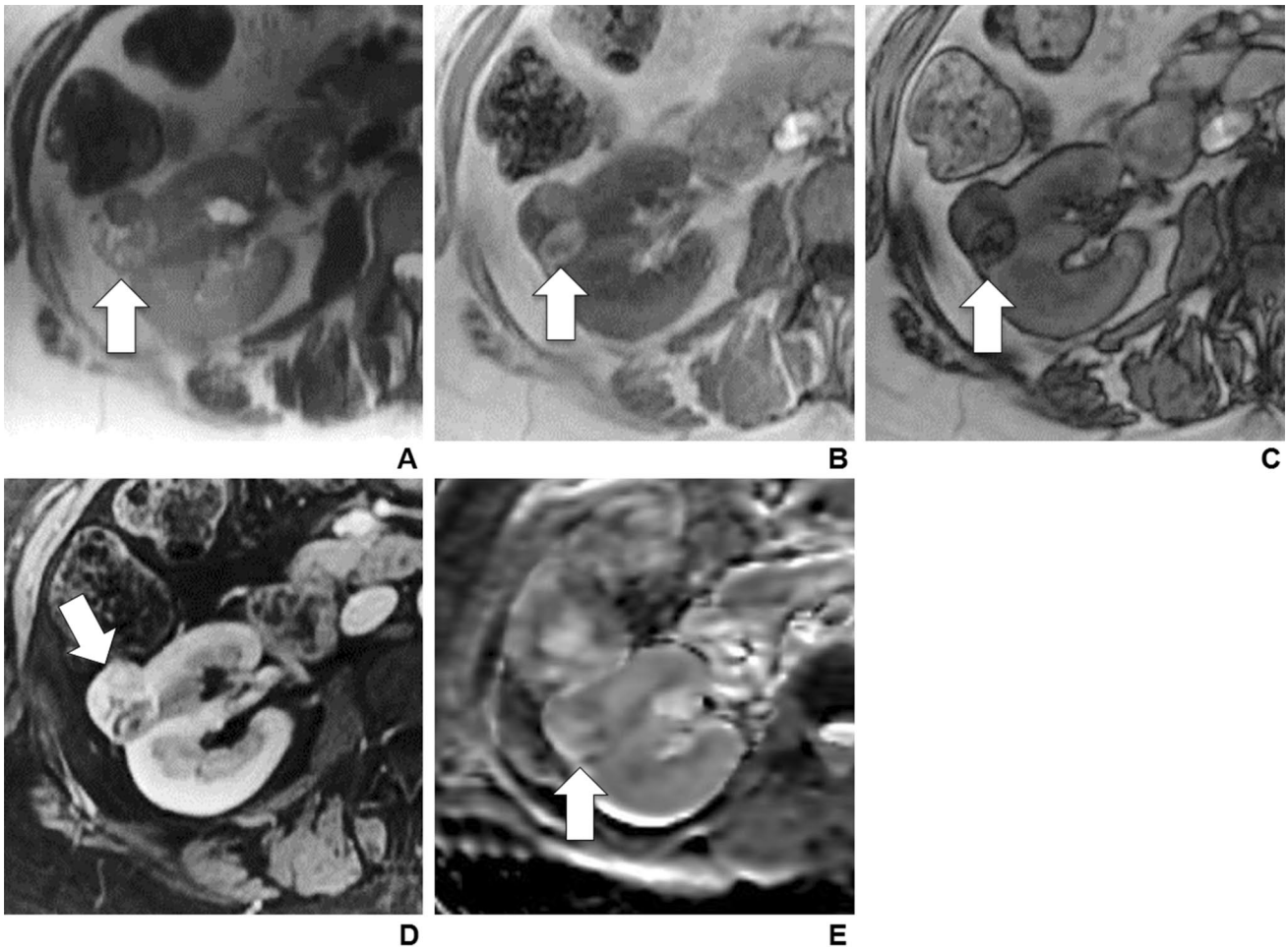

Fig. 3 A 46-year-old female with low-grade (ISUP Grade 1) clear cell RCC. **a** Axial T2W image shows a heterogeneously hyperintense mass in the interpolar region of the right kidney (white arrow) with predominantly increased T2W signal compared to the renal cortex. **b**, **c** Axial T1W in- and opposed-phase images show the presence of intratumoral microscopic fat (arrows) with signal intensity drop on opposed-phase compared to in-phase images. **d** Axial FS T1W post-gadolinium-enhanced image obtained in the corticomedullary phase depicts intense enhancement at the anterior aspect of the mass (arrow). **e** Axial ADC map image shows predominantly iso- to increased signal compared to the ipsilateral renal cortex

Statistical analysis

All data are presented as mean ± standard deviation with range provided. Demographic variables and subjective outcomes were compared using the Chi-square test of proportions, and parametric data were compared using multivariate analysis. Threshold p value < 0.05 indicated a statistically significant difference. Inter-observer agreement was assessed using Cohen's kappa statistic. Diagnostic accuracies were tabulated for categorical variables and assessed using receiver operator characteristic (ROC) curve analyses. For quantitative variables, the optimal cut-points for maximizing sensitivity and specificity of diagnosis were evaluated using Youden's method. Logistic regression modeling was performed for statistically significant variables. Statistical analysis was performed with STATA Data analysis and statistical software, version 13 (Foster City Station, Texas, USA).

Table 2 Subjective MRI features of T1a (< 4 cm) solid clear cell renal cell carcinoma

	ADC signal intensity relative to renal cortex[a]						Signal intensity drop on chemical shift MRI[b]				Homogeneity on nephrographic phase-enhanced MRI[c]			
	Radiologist 1			Radiologist 2			Radiologist 1		Radiologist 2		Radiologist 1		Radiologist 2	
	Hypo	Iso	Hyper	Hypo	Iso	Hyper	Present	Absent	Present	Absent	Homogeneous	Heterogeneous	Homogeneous	Heterogeneous
Low grade ($N=38$)	29.6% ($n=8/27$)	40.7% ($n=11/27$)	29.6% ($n=8/27$)	3.7% ($n=1/27$)	48.1% ($n=13/27$)	48.1% ($n=13/27$)	36.8% ($n=14/38$)	63.2% ($n=24/38$)	26.3% ($n=10/38$)	73.7% ($n=28/38$)	76.3% ($n=29/38$)	23.7% ($n=9/38$)	60.5% ($n=23/38$)	39.5% ($n=15/38$)
High grade ($N=11$)	62.5% ($n=5/8$)	12.5% ($n=1/8$)	25% ($n=2/8$)	62.5% ($n=5/8$)	12.5% ($n=1/8$)	25% ($n=2/8$)	0% ($n=0/11$)	100% ($n=11/11$)	0% ($n=0/11$)	100% ($n=11/11$)	54.5% ($n=6/11$)	45.4% ($n=5/11$)	45.4% ($n=5/11$)	54.5% ($n=6/11$)
p value[d]	0.194			0.065			0.017		0.057		0.159		0.374	
Inter-observer agreement[e]	0.34						0.67				0.32			

[a]Apparent diffusion coefficient signal intensity judged by evaluating the axial slice of the tumor, which contained the most solid enhancing components assessed by cross-referencing images with nephrographic phase-enhanced MRI. The darkest portion of the solid components was compared subjectively to the ipsilateral renal cortex

[b]Binary outcome: signal drop present or absent on opposed-phase compared to in-phase chemical shift MRI

[c]Homogeneity assessed using a 5-point Likert-type scale where 1 = completely homogeneous, 2 = mostly homogeneous, 3 = mixed areas of homogeneous and heterogeneous signal, 4 = mostly heterogeneous and 5 = completely heterogeneous. Scores of three or higher were considered to be markers of heterogeneity

[d]Comparisons performed using the Chi-square statistic

[e]Inter-observer agreement assessed using Cohen's kappa statistic

Results

There were no differences in age (59 ± 10 years for low grade vs. 52 ± 13 years for high grade, $p=0.098$), gender (15 females in the low-grade group and 6 females in the high-grade group, $p=0.374$), or size of tumors (23 ± 6 [16–36] mm for low grade vs. 27 ± 7 [range 15–36] mm for high grade, $p=0.137$) between groups. A summary of the results of subjective features studied is provided in Table 2. The only statistically significant feature which differed between low-grade and high-grade tumors was the presence of signal intensity drop on opposed-phase chemical shift MRI. After consensus review, it was established that 36.8% (14/38) low-grade tumors compared to zero (0/11) high-grade tumors demonstrated the presence of microscopic fat ($p=0.017$). Inter-observer agreement was moderate ($K=0.67$). Results from the consensus review indicate that the presence of microscopic fat on MRI was specific for diagnosis of low-grade disease (100.0% [71.5–100.0]) but with low sensitivity (36.8% [21.8–54.6]), Figs. 2 and 3. There were no differences in subjective assessment of ADC signal or tumor heterogeneity assessed subjectively for either radiologist ($p>0.05$) and inter-observer agreement was only fair ($K=0.34$ and 0.24 respectively); however, there was a trend towards lower ADC values in high-grade tumors for both radiologists.

A summary of the results for quantitative analyses are provided in Table 3. When comparing low-grade to high-grade tumors, the following features were all higher in low-grade compared to high-grade cT1a clear cell RCC; corticomedullary phase wash-in rate (i.e., degree of enhancement) ($p=0.015$), chemical shift signal intensity index ($p=0.138$), mean and tenth-centile ADC ($p=0.050$ and 0.049) with no difference in other variables studied between groups. The area under the ROC curve for each variable with optimal sensitivity and specificity for diagnosis of low-grade disease were wash-in rate, 0.77 (confidence intervals 0.62–0.91), 73.7% and 81.8% when > 157.0; chemical shift signal intensity index 0.65 (0.48–81), 65.3% and 68.6% when > 10.3%; tenth-centile ADC 0.75 (0.52–0.98), 73.3% and 75.0% when > 1.340 mm^2/s, Fig. 4. A logistic regression model combining microscopic fat (judged subjectively) with corticomedullary phase wash-in and tenth-centile ADC yielded an area under the ROC curve with optimal sensitivity and specificity for diagnosis of low-grade disease of 0.98 (0.94–1.0) with sensitivity/specificity 87.5%/100%, Fig. 5.

Discussion

This study evaluated the ability of MRI to differentiate between ISUP low-grade and high-grade cT1a clear cell renal cell carcinomas. Among subjective features studied, the presence of microscopic fat was highly specific for diagnosis of low-grade disease and showed moderate inter-observer agreement. Quantitative analysis showed that corticomedullary phase wash-in rate (degree of enhancement) and tenth-centile ADC differed between groups with low-grade tumors enhancing to a greater degree and showing higher tenth-centile ADC values. A logistic regression model combining microscopic fat with corticomedullary phase wash-in rate and tenth-centile ADC was highly accurate for diagnosis of low-grade tumors. Our preliminary results support previous studies that have shown that CT and MR radiomic features may differentiate between low-grade and high-grade CC-RCC and more specifically, in combination with the presence of microscopic fat validate these observations in < 4 cm solid clear cell RCC. These observations may be clinically relevant particularly when determining candidacy for active surveillance among < 4 cm solid clear cell RCC which may have been diagnosed on biopsy [14] or by using recently described accurate multi-parametric MR imaging algorithms [11, 34, 36].

Outwater et al. first described the phenomenon of signal intensity loss on opposed-phase compared to in-phase dual-echo chemical shift MRI in clear cell RCC due to the presence of intracytoplasmic or intracellular fat [37]. Though

Table 3 Quantitative MRI parameters of T1a (< 4 cm) solid clear cell renal cell carcinomas

	Low grade ($N=38$)	High grade ($N=11$)	p value[e]
Size (mm)	23 ± 6 (13–36)	27 ± 7 (15–36)	0.137
Chemical shift SI index[a]	7.0 ± 30.7 6.9 (−77.7 to 68.0)	0.1 ± 13.0 0.4 (−26.1 to 18.1)	0.138
Chemical shift adrenal-to-spleen SI ratio (SIR)[b]	93.1 ± 30.0	102.9 ± 13.3	0.296
Mean apparent diffusion coefficient (mm^2/s)	1.58 ± 0.29	1.28 ± 0.39	0.050
25th centile ADC (mm^2/s)	1.52 ± 0.29	1.24 ± 0.40	0.069
Tenth-centile ADC (mm^2/s)	1.59 ± 0.41	1.21 ± 0.43	0.049
Corticomedullary phase-enhanced wash-in rate[c]	289.4 ± 204.6	129.7 ± 81.5	0.015
Nephrographic phase-enhanced wash-out rate[d]	0.53 ± 1.6 0.20 (0.03–9.64)	0.34 ± 0.31 0.17 (0.06–1.06)	0.632

[a]Chemical shift signal intensity index = $[(SI_{tumorIP} - SI_{tumorOP})/SI_{TumorIP}] \times 100$

[b]Chemical shift Adrenal-to-Spleen SI Index = $[(SI_{tumorOP} - SI_{spleenOP})/(SI_{tumorIP} - SI_{spleenIP})] \times 100$

[c]Wash-in rate = ([[Corticomedullary phase signal intensity − Pre-contrast phase signal intensity]/Pre-contrast phase signal intensity] × 100)

[d]Wash-out rate = ([[Nephrographic phase signal intensity/Corticomedullary phase signal intensity]/Corticomedullary phase signal intensity] × 100)

[e]Comparisons performed using multivariate analysis

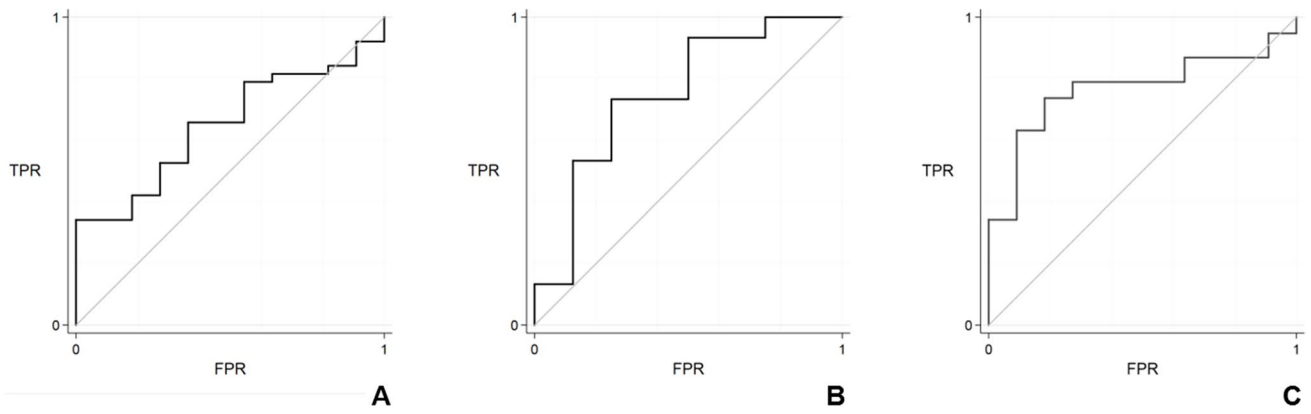

Fig. 4 Receiver operator characteristic curves for chemical shift signal intensity index (**a**). Tenth-centile ADC (**b**) and corticomedullary phase wash-in index (**c**) for differentiating low-grade from high-grade clear cell RCC. *TPR* true-positive rate (sensitivity) and *FPR* false-positive rate (1-specificity)

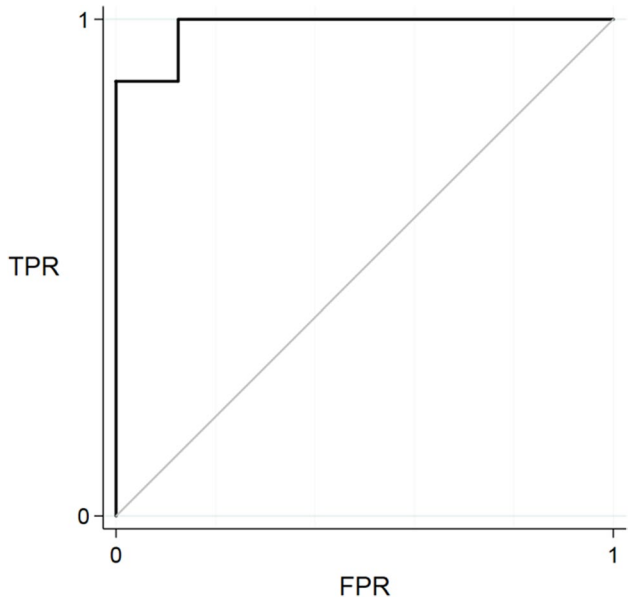

Fig. 5 Receiver operator characteristic curve for a logistic regression model combining the subjective impression of microscopic fat on chemical shift MRI, tenth-centile ADC, and corticomedullary phase wash-in index for differentiating low-grade from high-grade clear cell RCC

other RCC may also show "microscopic fat," suspected to be on the basis of clear cell heterogeneity among tumors [38], clear cell RCC and fat poor AML have been shown to have the highest amount of signal drop on chemical shift MRI [39]. Among clear cell tumors, to our knowledge, the presence of "microscopic fat" has not been evaluated in cT1a masses as a potential imaging marker for low-grade disease. Histologically, though the ISUP grading system relies primarily on nucleolar size [27], a commonly encountered finding occurs in tumors which progress from low grade to higher grade, which is a change from optically clear cytoplasm (due to abundant intracytoplasmic fat that is lost during processing) to optically pinkish cytoplasm (due to less fat content) [40]. In a prior study by Pedrosa and colleagues who performed histopathological analysis of clear cell RCC, the presence of fat could not differentiate between ISUP Grade 3 or 4 tumors; however, the authors did not evaluate the more clinically important question of low-grade (Grades 1 or 2) to high-grade (Grades 3 or 4) disease and did not evaluate cT1a tumors, which tend to show more homogeneous ISUP pattern throughout the tumor compared to cT2 or higher tumors which are more heterogeneous and composed of varying amounts of low-grade and high-grade disease [41]. In our study, the presence of microscopic fat was highly specific for diagnosis of low-grade disease and did not occur in T1a Grade 3 RCC.

Prior investigators have shown that high-grade clear cell RCC enhance to a lesser extent than low-grade tumors at multiphase imaging [17]. Our results confirm these findings in cT1a masses, as low-grade tumors had significantly higher corticomedullary phase wash-in compared to high-grade tumors. With respect to ADC, it has been consistently shown that ADC values are lower in the solid component of clear cell RCC with higher ISUP grade [42, 43]. Our study re-demonstrated these results and showed lower tenth-centile ADC values among high-grade tumors. We combined the statistically significant variables: microscopic fat, corticomedullary phase wash-in rate, and tenth-centile ADC into a logistic regression model that showed very high accuracy for diagnosis of low-grade tumors among T1a solid clear cell RCC. These results compare favorably to recent studies showing the combination of various radiomic features to be accurate for differentiation of clear cell grade on imaging [15, 19, 42–44].

Our study has limitations. The sample size is relatively small; in particular, the number of high-grade tumors in our cohort was limited; however, this can be expected since we only evaluated T1a tumors (higher ISUP Grade is more commonly found in >4 cm tumors [45, 46]). The high-grade group did not include any ISUP Grade 4 disease, which can also be expected in T1a tumors but is a limitation which may assess generalizability of our results to other patient populations. In our study, roughly one-fifth of cT1a clear cell tumors were high grade which is comparable to what has been previously reported, namely a prevalence of 20% high-grade or locally invasive tumors in cT1a lesions [47]. The MRI systems and techniques varied in our population, which may be considered a limitation for quantitative analyses in particular for ADC metrics and measured signal change on chemical shift MRI, but would also suggest an increased potential generalizability of our results. Though choice of b values for DWI varied slightly, ADC calculation for every study included low ($b<200$ mm^2/s) and high ($b>500$ mm^2/s), which partially mitigates influence of perfusion and diffusion effects between studies. The use of ADC histogram analyses, particularly when studying lower centile values, is a trade-off between detail and noise and future studies are required to validate the use of tenth versus higher centile assessment as more robust metrics to evaluate clear cell RCC grade. Future studies evaluating quantitative ADC in clear cell RCC should further evaluate reproducibility across systems and institutions. The combination of both 1.5T and 3T systems likely explains why the presence of microscopic fat was subjectively a significant variable differing between low-grade and high-grade tumors but quantitatively did not reach statistical significance. It has been previously shown that SI change on chemical shift MRI measured quantitatively differs by field strength [48]. We did not evaluate texture features quantitatively in this study, because the sample size was small, which limits the reliability of outcomes when testing the many texture

features available. Adding more variables to our tested logistic regression models would have also increased the risk of overfitting our models and overestimating the accuracy of diagnosis. These have previously described and validated in RCC and future studies might evaluate the incremental yield in accuracy of texture analysis in addition to the routinely acquired features evaluated in the present study.

In conclusion, this study validates previous work describing the ability of CT and MRI to differentiate between low-grade and high-grade clear cell RCC, but is potentially of higher clinical value because only cT1a tumors were included. Tumors measuring < 4 cm in size are increasingly managed with active surveillance and a priori knowledge of clear cell tumor subtype (through biopsy or more recently through highly accurate imaging algorithms on CT or MRI) combined with imaging features suggestive of high-grade disease may better stratify patients for radical therapy instead of surveillance. In our study, the combination of microscopic fat with higher corticomedullary phase wash-in rate and higher tenth-centile ADC values was highly accurate for diagnosis of low-grade disease. The immediate application of these findings into clinical practice is limited by the small sample size of the present study and use of quantitative analyses on MRI. Future studies are required to validate the ability of imaging features to diagnose and grade clear cell RCC on MRI, determine reproducibility, and assess the value of this information in clinical practice.

References

1. Gupta K, Miller JD, Li JZ, Russell MW, Charbonneau C. Epidemiologic and socioeconomic burden of metastatic renal cell carcinoma (mRCC): a literature review. Cancer Treat Rev 2008;34(3):193-205.
2. Jemal A, Siegel R, Xu J, Ward E. Cancer statistics, 2010. CA: a cancer journal for clinicians 2010;60(5):277-300.
3. Almassi N, Gill BC, Rini B, Fareed K. Management of the small renal mass. Transl Androl Urol 2017;6(5):923-930.
4. Volpe A, Cadeddu JA, Cestari A, et al. Contemporary Management of Small Renal Masses. European urology 2011;60(3):501-515.
5. Pierorazio PM, Hyams ES, Mullins JK, Allaf ME. Active surveillance for small renal masses. Reviews in urology 2012;14(1-2):13-19.
6. Lee H, Lee JK, Kim K, et al. Risk of metastasis for T1a renal cell carcinoma. World journal of urology 2016;34(4):553-559.
7. Cheville JC, Lohse CM, Zincke H, Weaver AL, Blute ML. Comparisons of outcome and prognostic features among histologic subtypes of renal cell carcinoma. The American journal of surgical pathology 2003;27(5):612-624.
8. Lim RS, McInnes MDF, Siddaiah M, Flood TA, Lavallee LT, Schieda N. Are growth patterns on MRI in small (< 4 cm) solid renal masses useful for predicting benign histology? European radiology 2018;28(8):3115-3124.
9. Ljungberg B, Bensalah K, Canfield S, et al. EAU guidelines on renal cell carcinoma: 2014 update. European urology 2015;67(5):913-924.
10. Wang R, Wolf JS, Wood DP, Higgins EJ, Hafez KS. Accuracy of Percutaneous Core Biopsy in Management of Small Renal Masses. Urology 2009;73(3):586-590.
11. Canvasser NE, Kay FU, Xi Y, et al. Diagnostic Accuracy of Multiparametric Magnetic Resonance Imaging to Identify Clear Cell Renal Cell Carcinoma in cT1a Renal Masses. J Urol 2017;198(4):780-786.
12. Dagher J, Delahunt B, Rioux-Leclercq N, et al. Clear cell renal cell carcinoma: validation of World Health Organization/International Society of Urological Pathology grading. Histopathology 2017;71(6):918-925.
13. Delahunt B, Cheville JC, Martignoni G, et al. The International Society of Urological Pathology (ISUP) grading system for renal cell carcinoma and other prognostic parameters. The American journal of surgical pathology 2013;37(10):1490-1504.
14. Marconi L, Dabestani S, Lam TB, et al. Systematic Review and Meta-analysis of Diagnostic Accuracy of Percutaneous Renal Tumour Biopsy. Eur Urol 2016;69(4):660-673.
15. Rosenkrantz AB, Niver BE, Fitzgerald EF, Babb JS, Chandarana H, Melamed J. Utility of the apparent diffusion coefficient for distinguishing clear cell renal cell carcinoma of low and high nuclear grade. AJR Am J Roentgenol 2010;195(5):W344-351.
16. Sun MR, Ngo L, Genega EM, et al. Renal cell carcinoma: dynamic contrast-enhanced MR imaging for differentiation of tumor subtypes--correlation with pathologic findings. Radiology 2009;250(3):793-802.
17. Vargas HA, Delaney HG, Delappe EM, et al. Multiphasic contrast-enhanced MRI: Single-slice versus volumetric quantification of tumor enhancement for the assessment of renal clear-cell carcinoma fuhrman grade. Journal of Magnetic Resonance Imaging 2012;37(5):1160-1167.
18. Huhdanpaa H, Hwang D, Cen S, et al. CT prediction of the Fuhrman grade of clear cell renal cell carcinoma (RCC): towards the development of computer-assisted diagnostic method. Abdominal imaging 2015;40(8):3168-3174.
19. Ding J, Xing Z, Jiang Z, et al. CT-based radiomic model predicts high grade of clear cell renal cell carcinoma. European journal of radiology 2018;103:51-56.
20. Lubner MG, Stabo N, Abel EJ, Del Rio AM, Pickhardt PJ. CT Textural Analysis of Large Primary Renal Cell Carcinomas: Pretreatment Tumor Heterogeneity Correlates With Histologic Findings and Clinical Outcomes. AJR Am J Roentgenol 2016;207(1):96-105.
21. Amin MB, Greene FL, Edge SB, et al. The Eighth Edition AJCC Cancer Staging Manual: Continuing to build a bridge from a population-based to a more "personalized" approach to cancer staging. CA: a cancer journal for clinicians 2017;67(2):93-99.
22. Edge SB, Compton CC. The American Joint Committee on Cancer: the 7th edition of the AJCC cancer staging manual and the future of TNM. Annals of surgical oncology 2010;17(6):1471-1474.
23. Takayama T, Sugiyama T, Kai F, et al. Characteristics of aggressive variants in T1a renal cell carcinoma. Journal of cancer research and clinical oncology 2011;137(11):1653-1659.
24. Schlomer B, Figenshau RS, Yan Y, Venkatesh R, Bhayani SB. Pathological features of renal neoplasms classified by size and symptomatology. The Journal of urology 2006;176(4 Pt 1):1317-1320; discussion 1320.
25. Bagrodia A, Darwish OM, Rapoport Y, Margulis V. Risk prediction in the management of small renal masses. Current opinion in urology 2012;22(5):347-352.
26. Tomaszewski JJ, Uzzo RG, Smaldone MC. Heterogeneity and renal mass biopsy: a review of its role and reliability. Cancer biology & medicine 2014;11(3):162-172.

27. Samaratunga H, Gianduzzo T, Delahunt B. The ISUP system of staging, grading and classification of renal cell neoplasia. Journal of kidney cancer and VHL 2014;1(3):26-39.
28. Schieda N, Thornhill RE, Al-Subhi M, et al. Diagnosis of Sarcomatoid Renal Cell Carcinoma With CT: Evaluation by Qualitative Imaging Features and Texture Analysis. AJR Am J Roentgenol 2015;204(5):1013-1023.
29. Zhang Y, Udayakumar D, Cai L, et al. Addressing metabolic heterogeneity in clear cell renal cell carcinoma with quantitative Dixon MRI. JCI Insight 2017;2(15).
30. Ramamurthy NK, Moosavi B, McInnes MD, Flood TA, Schieda N. Multiparametric MRI of solid renal masses: pearls and pitfalls. Clin Radiol 2014.
31. Sasiwimonphan K, Takahashi N, Leibovich BC, Carter RE, Atwell TD, Kawashima A. Small (<4 cm) renal mass: differentiation of angiomyolipoma without visible fat from renal cell carcinoma utilizing MR imaging. Radiology 2012;263(1):160-168.
32. Hindman N, Ngo L, Genega EM, et al. Angiomyolipoma with minimal fat: can it be differentiated from clear cell renal cell carcinoma by using standard MR techniques? Radiology 2012;265(2):468-477.
33. Karlo CA, Donati OF, Burger IA, et al. MR imaging of renal cortical tumours: qualitative and quantitative chemical shift imaging parameters. Eur Radiol 2013;23(6):1738-1744.
34. Cornelis F, Tricaud E, Lasserre AS, et al. Routinely performed multiparametric magnetic resonance imaging helps to differentiate common subtypes of renal tumours. Eur Radiol 2014;24(5):1068-1080.
35. Schieda N, Dilauro M, Moosavi B, et al. MRI evaluation of small (<4cm) solid renal masses: multivariate modeling improves diagnostic accuracy for angiomyolipoma without visible fat compared to univariate analysis. Eur Radiol 2015.
36. Kay FU, Canvasser NE, Xi Y, et al. Diagnostic Performance and Interreader Agreement of a Standardized MR Imaging Approach in the Prediction of Small Renal Mass Histology. Radiology 2018;287(2):543-553.
37. Outwater EK, Bhatia M, Siegelman ES, Burke MA, Mitchell DG. Lipid in renal clear cell carcinoma: detection on opposed-phase gradient-echo MR images. Radiology 1997;205(1):103-107.
38. Lopez JI, Angulo JC. Pathological Bases and Clinical Impact of Intratumor Heterogeneity in Clear Cell Renal Cell Carcinoma. Curr Urol Rep 2018;19(1):3.
39. Krishnan B, Truong LD. Renal epithelial neoplasms: the diagnostic implications of electron microscopic study in 55 cases. Human pathology 2002;33(1):68-79.
40. Sayeed S, Lindsey KG, Baras AS, et al. Cytopathologic features of clear cell papillary renal cell carcinoma: A recently described variant to be considered in the differential diagnosis of clear cell renal epithelial neoplasms. Cancer cytopathology 2016;124(8):565-572.
41. Pedrosa I, Chou MT, Ngo L, et al. MR classification of renal masses with pathologic correlation. European radiology 2008;18(2):365-375.
42. Parada Villavicencio C, Mc Carthy RJ, Miller FH. Can diffusion-weighted magnetic resonance imaging of clear cell renal carcinoma predict low from high nuclear grade tumors. Abdominal radiology (New York) 2017;42(4):1241-1249.
43. Woo S, Suh CH, Kim SY, Cho JY, Kim SH. Diagnostic Performance of DWI for Differentiating High- From Low-Grade Clear Cell Renal Cell Carcinoma: A Systematic Review and Meta-Analysis. AJR Am J Roentgenol 2017;209(6):W374-W381.
44. Mytsyk Y, Dutka I, Borys Y, et al. Renal cell carcinoma: applicability of the apparent coefficient of the diffusion-weighted estimated by MRI for improving their differential diagnosis, histologic subtyping, and differentiation grade. International urology and nephrology 2017;49(2):215-224.
45. Tabibi A, Parvin M, Abdi H, Bashtar R, Zamani N, Abadpour B. Correlation between size of renal cell carcinoma and its grade, stage, and histological subtype. Urology journal 2007;4(1):10-13.
46. Thompson RH, Kurta JM, Kaag M, et al. Tumor size is associated with malignant potential in renal cell carcinoma cases. The Journal of urology 2009;181(5):2033-2036.
47. Campbell S, Uzzo RG, Allaf ME, et al. Renal Mass and Localized Renal Cancer: AUA Guideline. The Journal of urology 2017;198(3):520-529.
48. Ream JM, Gaing B, Mussi TC, Rosenkrantz AB. Characterization of adrenal lesions at chemical-shift MRI: a direct intraindividual comparison of in- and opposed-phase imaging at 1.5 T and 3 T. AJR Am J Roentgenol 2015;204(3):536-541.